行政院國家科學委員會專題研究計畫　成果報告

由共振腔結構決定非線性雷射動力學研究(3/3)

計畫類別：個別型計畫
計畫編號：NSC92-2112-M-009-037-
執行期間：92 年 08 月 01 日至 93 年 07 月 31 日
執行單位：國立交通大學光電工程研究所

計畫主持人：謝文峰
共同主持人：程思誠

報告類型：完整報告

處理方式：本計畫涉及專利或其他智慧財產權，1 年後可公開查詢

中　華　民　國 93 年 11 月 1 日

附件一

行政院國家科學委員會補助專題研究計畫 ☒ 成 果 報 告 □期中進度報告

由共振腔結構決定非線性雷射動力學研究(3/3)

計畫類別：☒ 個別型計畫　　□ 整合型計畫
計畫編號：NSC92-2112-M-009-037
執行期間： 92 年 08 月 01 日至 93 年 07 月 31 日

計畫主持人：謝文峰
共同主持人：程思誠
計畫參與人員：

成果報告類型(依經費核定清單規定繳交)：☒精簡報告　□完整報告

本成果報告包括以下應繳交之附件：
□赴國外出差或研習心得報告一份
□赴大陸地區出差或研習心得報告一份
□出席國際學術會議心得報告及發表之論文各一份
□國際合作研究計畫國外研究報告書一份

處理方式：除產學合作研究計畫、提升產業技術及人才培育研究計畫、列管計畫及下列情形者外，得立即公開查詢
□涉及專利或其他智慧財產權，□一年□二年後可公開查詢

執行單位：國立交通大學光電工程研究所

中　華　民　國 93 年 10 月 26 日

行政院國家科學委員會專題研究計畫成果報告

由共振腔結構決定的非線性雷射動力學研究(3/3)

Resonator configuration dependent nonlinear laser dynamics (3/3)

計畫編號：NSC 92-2112-M-009-037-
執行期限：92 年 8 月 1 日至 93 年 7 月 31 日
主持人：謝文峰教授　　國立交通大學光電工程研究所

一、中文摘要

在本報告中我們研究端面幫浦 Nd:YVO_4 雷射操作在簡併共振腔結構(如 g_1g_2=1/4)附近支共振腔結構相關的不穩定與渾沌現象。我們發現雷射的不穩現象發生在簡併位置兩側之很窄的區域內，並以週期、週期加倍、和渾沌時間的變遷的形式展現。利用柯林基分和速率方程式，並考慮熱透鏡效應，我們展示模擬與實驗結果相當吻合。這個結果為第一次報導熱透鏡效應如何影響雷射不穩現象。

關鍵詞：雷射、共振腔、光渾沌現象、固態雷射。

Abstract

We experimentally studied the cavity-configuration-dependent instability in an end-pumped Nd:YVO_4 laser in the vicinity of the degenerate resonator configuration of g_1g_2 = 1/4 with small pump size. We found the laser instability occurs in a very narrow range of cavity tuning on each side of the degeneracy that shows periodic, period-doubling, and chaotic time evolution. By using Collin's integral and the rate equation with taking into account the thermal lens effect, we show the simulation consistent with the experiment. As far as we know, the observed instabilities are new and this is the first report to discuss the relationship between the instability and the thermal lens effect.

Keywords: Laser, Resonator, Optical Chaos, Solid-State Laser.

二、緣由與目的

It is commonly believed that spontaneous instabilities are impossible in class B lasers described by simple two-level rate equations without additional degree of freedom such as external modulation, light injection, delayed feedback, etc. [1]. However, the transverse effect such as gain variation and diffraction in the resonator supports the additional degree of freedom and has been demonstrated playing important roles in lasers [2,3]. Because various transverse modes may be excited especially when the laser is operated at near-degeneracy, a degenerate resonator is thus a good choice for obtaining a chaotic laser output. Previously, we have analyzed an iterative map of q-parameter of the resonator [4] and obtained that a laser will become unstable near some degenerate cavity configurations under persistent nonlinear effects. In an end-pumped cw Nd:YVO_4 laser, we have studied very different laser behaviors under different pump sizes [5,6]

when the cavity is near the 1/3-transverse degeneracy (g_1g_2 = 1/4). Recently, the Petermann K factor has also been calculated maxima on each side of the degeneracy under strong gain guiding or small pump size [7]. It is emphasized in the vicinity of the degeneracies the empty-cavity degenerate transverse modes are phase-locked and the resultant radial phase profile strongly depends on the cavity length detuning.

In this report, we study the cavity-configuration-dependent instability and determine the unstable regions with cavity length, pump power, and pump size as the control parameters. When the pump size is small, we found the laser always exhibits stable cw output except for a very narrow range of cavity tuning on each side of the degeneracy. The temporal behavior of the laser output shows periodic, period-doubling, and chaotic evolution. We also observed very different far-field patterns when we scanned the cavity length. In particular, an anomalous mode pattern is accompanied with frequency beating very close to the degeneracy. The simulation in use of Collin's integral and rate equation with taking into account the thermal lens effect shows good agreement with the experiment.

三、研究方法與步驟

A. Experiment

The experimental setup is schematically shown in Fig. 1. The laser consists of a 1-mm thick Nd:YVO_4 laser crystal whose one end face acts as an end mirror and a spherical mirror with radius of curvature of 8 cm as the output coupler (OC). A cw near-TEM_{00} Ti-sapphire laser at wavelength of 808 nm was used as the pump source that was focused by a collimating lens onto the crystal such that the pump size is adjustable. The end face of the crystal as the end mirror faced toward the pump beam has a dichroic coating with greater than 99.8% reflection at 1.064 μm and greater than 99.5% transmission at 808 nm; the other end face comprised an antireflection layer at 1.064 μm to avoid the effect of intracavity etalons. The OC of 10% transmission was mounted upon a translation stage so we could tune the cavity length L near the degenerate configuration. The degeneration point of g_1g_2 = 1/4 which corresponds to L = 6 cm is determined by the cavity length where the lowest lasing threshold occurs [8]. The laser output was split into two beams, one of which was recorded by a CCD camera and the other was further split into two beams that was individually collected by two photodiodes (PDs) with rise time < 0.3 ns. The signals of PDs were then fed into a LECROY-9450A oscilloscope (bandwidth 200 MHz) and an HP8560E RF spectrum analyzer (bandwidth 2.9 GHz), respectively. The Gaussian pump radius, w_p, is determined by the standard knife method.

B. Simulation

In order to understand the cavity-dependent instability, we numerically simulated this laser system by using Collin's integral [9] together with the rate equation as described in our previous work [6]. The model is able to describe a single-longitudinal multi-transverse mode laser [10] and was used to analyze the decay rate of standing-wave laser cavities [11]. In our system the cylindrically symmetric resonator and the thin slab gain medium were assumed. We did not consider the dispersion of the active medium or frequency detuning between the atomic transition and the cavity mode, so that the gain is assumed to be real. Given an initial gain distribution and

electric field, the field evolution will converge to a stationary solution if the final state is stable cw. Contrarily, if the final state is unstable, the electric field will automatically evolve to a dynamical state. When the thermal lens effect was considered, we imposed a radial phase distribution in the diffraction integral from Eqs. (2), (6), and (11) of Ref. 12. The thermal induced stress, the thermal deformation of the crystal, and the thermal fluctuation were neglected. To obtain the time evolution of the output power, we set the reference plane with 600-μm aperture at the flat end mirror and laterally integrated the intensity profile each round trip. The parameters used are the stimulated emission cross section of 25×10^{-19} cm^2, the spontaneous decay rate of 2×10^4 s^{-1}, the saturation parameter of the active medium of 1.12×10^{10} J/F m^{-2}, the fractional thermal loading of 0.23, the absorption coefficient of the laser crystal of 1930 m^{-1}, the thermal conductivity of 5.23 $Wm^{-1}K^{-1}$, the thermal-optic coefficient of 8.5×10^{-6} K^{-1}, and the others are the same as described in the experiment.

四、結果與討論

A. Experiment

The output power varying with the cavity length under different pump radii is shown in Fig. 2(a). The bottom three curves for w_p = 19 μm show that a higher pump power not only widens but also heightens the power hump. The laser exhibits stable cw for almost entire range of the studied 3-mm cavity tuning. However, within a narrow range of L on each side of the power hump, denoted as stars in the Fig. 2(a), we can always observe the spontaneous instabilities. The top two curves are the cavity-length dependence of output power for w_p = 25 and 34 μm at pump power of 300 mW, in which the triangles and the solid circles denote the unstable regions for both cases. Note that the radius of the cold-cavity fundamental mode is approximately 108 μm. Summarized in Fig. 2(b) are the unstable regions in terms of the cavity length and the pump power for three pump sizes of 19, 25, and 34 μm. We used single symbol to denote a narrow unstable region while used twin symbols to encompass a wider unstable region around 100 μm. We see the unstable regions on the short-cavity side are well separated for different w_p and located farther away from the degeneracy with increasing the pump power; contrarily, those on the long-cavity side are located very close to the degeneracy and nearly independent of the pump power.

When the cavity length is tuned from the long-cavity side toward and across the degeneracy, various far-field mode patterns can be observed. The mode pattern shows near fundamental Gaussian distribution far from the degeneracy. Tuning L close to the right edge of the unstable region, we observed a slightly distorted mode pattern. When the cavity is set within the unstable region of about 100 μm, the mode pattern becomes non-cylindrically symmetric and seriously spreads in a special direction as shown in Fig. 3(a). This anomalous spreading pattern maintains wider than the whole unstable region by few tens of micrometers. When L is tuned across the range showing the spreading pattern, the far-field pattern recovers to a cylindrically symmetric one but turns to many concentric rings with a dark center that is the far-field pattern of the multi-beam-waist mode [6]. Further tuning L toward the unstable region on the short-cavity side, we observed the cylindrically symmetric mode pattern as shown in Fig. 3(b) that differs from those in the unstable region of the long-cavity side as in Fig. 3(a).

We further investigated the temporal behavior of the output power within the unstable regions at P_{pump} = 260 mW and w_p = 34 μm. Figure 4(a) shows a periodic time trace when the cavity is tuned at the edge of the long-cavity unstable region. Its corresponding RF spectrum in Fig. 4(b) shows one main peak at 1.33 MHz and three harmonics. When the cavity length is decreased by ~20 μm from the position of Fig. 4(a), a period-2 evolution was observed with its time trace and spectrum shown in Fig. 4(c) and 4(d), respectively. Continuing on decreasing the cavity length, we recorded a chaotic evolution in Fig. 4(e) with broad low frequency spectrum in Fig. 4(f). The calculation in use of chaos data analyzer (American Institute of Physics) shows the embedding dimension of the chaotic evolution is approximately 2.1.

Although the details of the instabilities on both sides of degeneracy may be different but they are closely related to high order transverse modes because the instabilities disappear when a knife edge was inserted into the cavity beam by ~500 μm to inhibit the high order transverse modes, the high frequency responses of the cavity-configuration dependent instabilities are quite different on each side of degeneracy. On the long cavity side, we observed multiple beating frequencies at 812 MHz, 1.63 GHz, and 2.44 GHz [see Fig. 4(g)] that was confirmed with a Febry-Perot interferometer (FPI) having FSR = 15 GHz and finesse = 150. It results from simultaneously exciting the Laguerre-Gaussian $LG_{1,0}$ and/or $LG_{2,0}$ modes and reveals spatio-temporal instability, where, the subscripts 1 and 2 are the radial indices and 0 is the azimuthal index. However, within the short-cavity unstable region the spectrum shows only the longitudinal mode beating of 2.44 GHz. The mode profile may consist of frequency locked near-degenerate transverse modes (e.g. $LG_{q,0,0}$ and $LG_{q-2,3,0}$, where q is the longitudinal mode index). Thus, the transverse frequency beating is absent in both of the RF and the FPI spectra and it appears low frequency temporal instability within the short cavity unstable region.

To investigate the distinction between the instabilities on the long-cavity and the short-cavity sides, we use two PDs at different transverse positions to simultaneously record the laser power. The first PD is fixed at the center of the profile as the reference and the second PD is located at an off-axis position. When these two detectors are separated within a distance, their temporal traces on the oscilloscope are completely the same as shown in Fig. 5(a). However, we found on the long cavity side the temporal traces of larger separation exhibit anti-phase pulsing as shown in Fig. 5(b) that shows the higher peak of one trace coincides with the lower peak of the other trace. It indicates that it is multi-mode instability on the long-cavity side. On the other hand, within the short cavity unstable region, we always observe the in-phase behavior between two signals no matter at what position the second PD is located. It exhibits pure temporal instability.

B. Simulation

Figure 5(a) shows the output power as a function of L with considering the thermal lens effect. The curves of output power labeled as triangles, empty squares, and solid circles for w_p = 25, 30, and 35 μm respectively also show asymmetric power humps with respect to the degeneracy. The dependence of the power hump on w_p and P_p (the effective pump power) are the same as in Fig. 2(a). The unstable regions are summarized for four values of w_p in Fig. 5(b) which are similar to those in Fig. 2(b) except that the vertical axis of Fig. 5 is the effective pump power that matches with the

pump efficiency of ~0.6 taken from the measured pumping. Again, in Fig. 5(b) we used single symbol to denote a narrow unstable region while used twin symbols to encompass a wider unstable region. It shows similar unstable regions and dependence on w_p and P_p as those in Fig. 2(b); for example, at $w_p = 35$ μm, the unstable region shifts approximately from L = 5.94 to 5.90 cm on the short-cavity side as increasing the effective pump power that matches with the experiment data in Fig. 2(b). Moreover, the far-field intensity profiles beside the long-cavity unstable region are similar to those in Fig. 2(b) of Ref. 6. In addition, no instability can be observed as $w_p > 40$ μm, that is also consistent with the experiment.

To look into the influence of the thermal lens effect, we repeated the simulation without considering the thermal lens effect to determine the cavity-dependent output power and the unstable regions in Figs. 7(a) and 7(b). As compared with Fig. 5, we found the thermal lens effect leads to some phenomena: (1) an asymmetrical shape of the power hump; (2) asymmetrical unstable regions with respect to the degeneration point; (3) dependence of region shift on P_p for the short-cavity side but not the long-cavity side; and (4) much less shift of power maximum than shift of the unstable region (e.g., see $w_p = 30$ μm and $P_p = 150$ mW).

Without the thermal lens effect, not only the power hump but also the dynamical behaviors are symmetric with respect to the degeneracy. Since the beating frequency between the near-degenerate LG modes are absent on both long- and short-cavity instabilities, the frequencies of the near-degenerate LG modes are locked to one another. Therefore the frequency-locked modes, a supermode [14], that interacts with the inverted population and leads to the short-cavity instabilities. However, the long-cavity instabilities arise mainly from the frequency beating between the supermode and the other LG modes. Although the asymmetric (spreading) mode pattern of Fig. 3(a) is unable to be produced by using the cylindrically symmetric model with single optical frequency, the simulated results agree with the experiment of transverse mode beating. As far as we know, this is the first report that discusses the relationship between the instability and the thermal lens effect.

Furthermore, when the aperture on the reference plane is decreased to 450 μm, consistently with the experiment described before, the instability disappears. The stationary mode now consists of the near-degenerate LG modes with the same frequency but lack of the higher order $LG_{15,0}$ and $LG_{18,0}$ modes. This fact of transverse mode locking is confirmed from the absence of the transverse mode beating and from the observation of the intensity profile variation with the propagation distance as done in Ref. 6. The supermode lack of the components of the $LG_{15,0}$ and $LG_{18,0}$ modes is unable to arise the instability. Inserting a knife edge into the cavity beam in our experiment also result in a cylindrically symmetric pattern instead of a spreading pattern. Apparently, the high order modes with small amplitude may play an important role in symmetry breaking as indicated in Ref. 13. However, the origin of the symmetry breaking is still unknown.

五、結論

We have found the cavity-configuration-dependent instabilities and determined the two sets of the unstable regions beside the degeneracy near $g_1g_2 = 1/4$ in an end-pumped Nd:YVO_4 laser with small pump sizes. We illustrated the temporal behavior of the instabilities including the

chaotic output with low-dimension. The different far-field patterns beside the unstable regions are observed; in particular, a special spreading mode pattern is observed in the vicinity of the degeneracy. Our numerical results using cylindrically symmetric model with single frequency agree well with the experiments and reveal the influence of the thermal lens effect.

六、自我評估

在此三年期計畫中我們添購了倍頻 Nd:YVO_4 雷射作為鈦藍寶石雷射之幫浦源，提高幫浦雷射之穩定性，釐清幫浦不穩造成雷射渾沌現象研究上干擾之疑慮。上年度變更計劃採購氬離子雷射管和量測單模雷射波長所需之干涉儀。前者作為另一項超快雷射源從事光電材料之光電性質研究，也有相當不錯之成果發表；而後者，我們使用干涉儀確定所提出的新型多回徑本徵模或多光腰模之雷射輸出的確為單頻。真正物理內涵其實為由簡併之低階橫模鎖頻形成所謂「超模」 (supermode)。這年度(本計劃第三期)計劃中，我們利用適當的幫浦光斑和內腔光腰之控制，可以順利產生所謂的「瓶光束」(optical bottle beam)。這種光束目前需要用複雜的全像或光束干涉來得到。利用此光束可以用於原子捕捉於低光場區，以便減少對光束之干擾之優點。綜合這個三年計畫我們研究了諧頻鎖模與脈衝分裂現象，為共振腔結構相關之動態不穩定行為。到這三年來共發表 23 篇 SCI 論文，其中有關雷射動力學研究計 5 篇，其他 18 篇為有關光電材料之物理性質研究，成果還算不錯。

七、參考文獻

[1] C.O. Weiss, R. Vilaseca, Dynamics of lasers (VCH, New York, 1991).

[2] L.A. Lugiato, F. Prati, L.M. Narducci, P. Ru, J.R. Tredicce, D.K. Bandy, Phys. Rev. A 37 (1988) 3847.

[3] L.A. Lugiato, G.L. Oppo, J.R. Tredicce, L.M. Narducci, M.A. Pernigo, J. Opt. Soc. Am. B 7 (1990) 1019.

[4] M.D. Wei, W.F. Hsieh, C. C. Sung, Opt. Commun. 146 (1998) 201.

[5] C.H. Chen, M.D. Wei, W.F. Hsieh, J. Opt. Soc. Am. B 18 (2001) 1076.

[6] C.H. Chen, P.T. Tai, M.D. Wei, W.F. Hsieh, J. Opt. Soc. Am. B 20 (2003) 1220.

[7] C.F. Maes, E.M. Wright, Opt. Lett. 29 (2004) 229.

[8] H.H. Wu, W.F. Hsieh, J. Opt. Soc. Am. B 18 (2001) 7.

[9] S.A. Collins, J. Opt. Soc. Am. 60 (1970) 1168.

[10] F. Hollinger, Chr. Jung, J. Opt. Soc. Am. B 2 (1985) 218.

[11] Y.J. Cheng, P.L. Mussche, A.E. Siegman, IEEE J. Quantum Electron. 31(1995) 391.

[12] M.E. Innocenzi, H.T. Yura, C.L. Fincher, R.A. Field, Appl. Phys. Lett. 56 (1990) 1831.

[13] E.J. D'Angelo, C. Green, J.R. Tredicce, N.B. Abraham, S. Balle, Z. Chen, G.L. Oppo, Physica D 61 (1992) 6.

[14] H. Lin, N.B. Abraham, Opt. Commun. 79 (1990) 476.

[15] W. Gadomski, B. Ratajska-Gadomska, J. Opt. Soc. Am. B 17 (2000) 188.

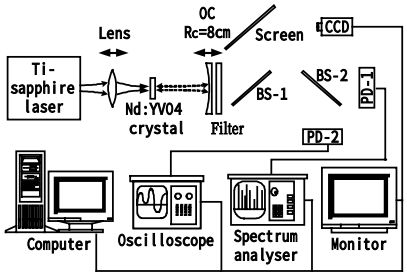

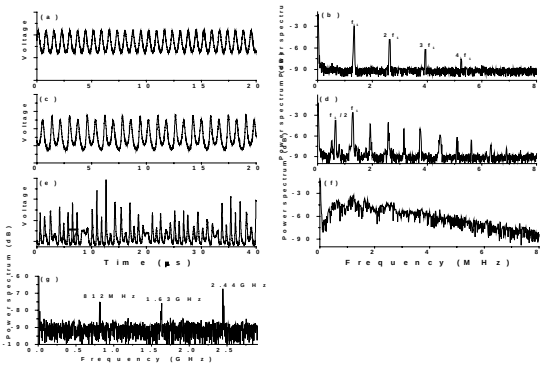

Fig. 1. The schematic of experimental set up. BS is the beam splitter.

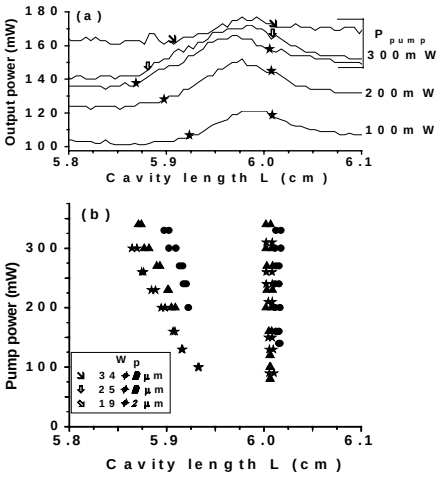

Fig. 2. The observed output power as a function of cavity length (a) and the unstable regions in terms of the cavity length and the pump power for different w_p (b). The symbols for w_p are the same in (a) and (b). The output power is around 40 mW for P_{pump} = 100 mW as w_p = 19 μm. Note that we have added 50 mW and 75 mW for the curves of P_{pump} = 200 mW and P_{pump} = 100 mW. The absorption efficiency of P_{pump} is about 60 - 70%. The lasing threshold is about 5 – 30 mW depending on L and w_p.

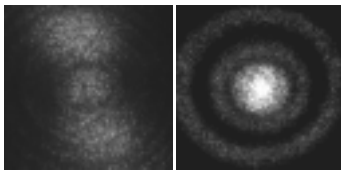

Fig. 3. The far-field mode patterns inside the long-cavity unstable region (a) and inside the short-cavity unstable region (b).

Fig. 4. The temporal evolution of laser output. (a) periodic, (c) period-doubled, and (e) chaotic output within the long-cavity unstable region. The RF spectra (b), (d), and (f), that correspond to (a), (c), and (e), respectively. (g) The high frequency RF spectrum of the spreading mode pattern of Fig. 3(a).

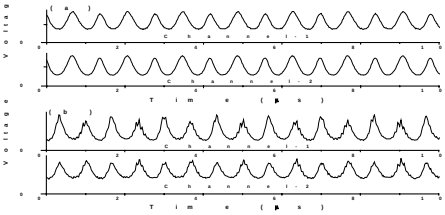

Fig. 5. The time traces in oscilloscope when the two PDs are separated close to each other (a) and farther away (b) for the long-cavity instabilities.

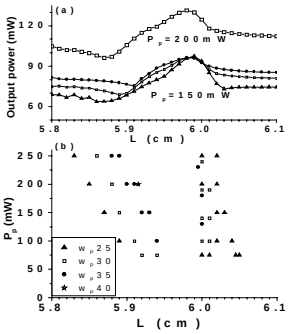

Fig. 6. The numerical output power as a function of cavity length with considering the thermal lens effect (a) and the unstable regions (b) for different w_p. The symbols for w_p are the same for (a) and (b).

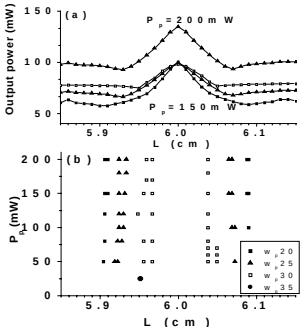

Fig. 7. The numerical output power as a function of cavity length (a) and the unstable regions (b) without considering the thermal lens effect. The symbols for w_p are the same for (a) and (b).